Chemo-Divergent Nickel(0)-Catalyzed Arene C–F Activation with Alkynes: Unprecedented C-F/C-H Double-Insertion

Lorena Capdevila[†], Tjark H. Meyer[‡], Steven Roldán-Gómez[†], Josep M. Luis[†], Lutz Ackermann*[‡], and Xavi Ribas*[†]

[†] Institut de Química Computacional i Catàlisi (IQCC) and Dep. Química, Universitat de Girona, Campus de Montilivi, E-17003, Girona, Catalonia, Spain.

[‡] Institut für Organische und Biomolekulare Chemie, Georg-August-Universität, Tammanstrasse 2, 37077 Göttingen, Germany

ABSTRACT: Nickel-catalyzed C-F activations enabled chemo-divergent C-C formation with alkynes by chelation assistance. The judicious choice of the alkynes electronic properties allowed the selective synthesis of double-insertion aromatic homologation or alkyne mono-annulation products by C-F/C-H activation. Based on the unambiguous crystallographic characterization of an unprecedented 9-membered nickelocyclic intermediate and extensive DFT studies, a plausible mechanistic rationale was established for the selective C-F activation and the chemo-divergent catalysis.

INTRODUCTION

Fluorinated compounds are key structural moieties in numerous areas of chemistry, with transformative applications to crop protection, catalysis, medicine and material sciences.[1-4] The introduction of fluorinated motifs thus changes the physical, chemical and biological properties of a given molecule, and in the pharmaceutical industry context, improves the stability and lifetime of F-containing pharmaceuticals, 50% feature aryl fluorides. However, the stability is often too pronounced and the lead compound is frequently poorly biodegradable. Therefore, it is desirable to develop new sustainable methods for the functionalization of aromatic C-F bonds, as an enabling strategy to establish novel chemo- and regio-selective transformation of fluorinated arenes. Transition metal-catalysed Ar–F functionalization is considerably more challenging than classical Ar-H or Ar–Hal (Hal = I, Br, Cl) activation, generally showing low selectivities and requiring electronically biased polyfluorinated substrates.[5-7] In particular, C–C formation reaction via C–F cleavage of fluoroarenes using nickel catalyst has been reported for Kumada-Corriu,[8-16] Suzuki-Miyaura[17-22] and Negishi[23] cross-coupling reactions. However, all these methods use activated aryl nucleophiles, such as highly reactive Grignard reagents, zincates and boronic acids as the coupling partner for C–C formation via transmetallation (Scheme 1a). Alkyne insertion reactions have emerged as a powerful tool for the formation of cyclic compounds. Thus, several protocols through transition metal-catalyzed C–H activation have been established with alkynes to form isoquinolones[24-28] or indoles.[29-32] The use of alkyne as a coupling partner can also lead to the direct formation of polysubstituted arenes.[33-36] In this context, Chatani[37] and Huang[38] recently reported nickel-catalyzed[39] aromatic homologation reaction by a double C-H bond activation using 8-aminoquinoline as the directing group (Scheme 1b).

Taking into account the steadily increasing interest in the functionalization of the strongest bonds with carbon, we sought to develop new nickel(0)-catalyzed cyclizations of fluorinated arene via alkyne insertion reactions.[40] Herein, we show that catalytic quantities of $Ni(COD)_2$ enable the chemo-divergent C-F activation over C-H activation of fluoroarenes bearing either pyrimidin-2-amine[29, 41] or 8-aminoquinoline[42] groups, towards isoquinolones and polysubstituted arenes. Mechanistic investigations were performed to clarify the parameters that control the chemo-selectivity. Furthermore, the use of the 8-aminoquinoline group allowed us to isolate an unprecedented organometallic nickel(II) metalacycle featuring a doubly inserted acetylene, as the key intermediate in the aromatic homologation strategy (Scheme 1c).[43]

Scheme 1. (a) Nickel-catalyzed C–F activation reactions using highly reactive, preactivated R-M nucleophiles. (b) Alkyne annulation via C–H activation by nickel catalysts. (c) Nickel-catalyzed C–F functionalization with internal alkynes.

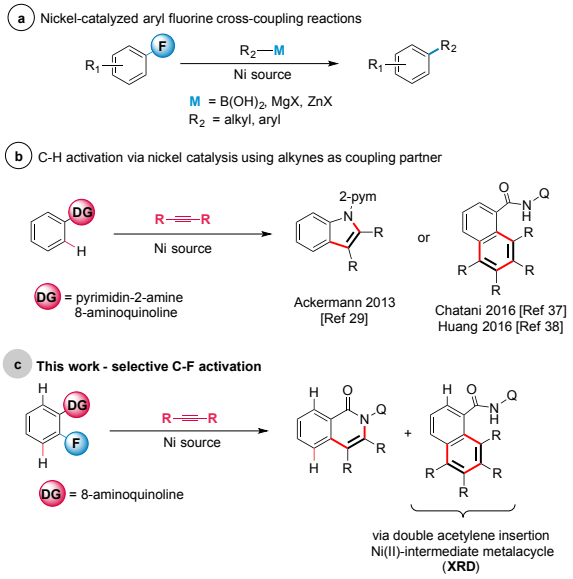

RESULTS

Role of N-substitution pattern. Initially, we probed the catalytic activation of the strong C–F bond by exploring the role of the directing group (DG) nature in the reaction with diphenylacetylene. To this end, we used substrates with two different well-studied directing groups, namely bidentate 8-aminoquinoline **1a** and monodentate pyrimidin-2-amine **1d** (Scheme 2). When the reaction was carried out with substrate **1d**, a sluggish alkyne annulation reaction via C–H activation took place (**3da**, 18%), and the C–F bond remained intact. However, the use of 8-aminoquinoline as a bidentate directing group was crucial for the selective functionalization of the stronger C–F bond. Based on considerable optimization (Table S1), the alkyne mono-annulation product (**3aa**) was obtained in a 17% yield, and the aromatic homologation product (**2aa**) was formed in a 63% yield (Scheme 2). This preliminary result clearly suggested that a) the bidentate 8-AQ was ideal for the selective C–F cleavage whereas the monodentate DG only shows residual reactivity on C-H activation, and b) the insertion of two alkynes rendering the aromatic homologation product by dual C-F/C-H activation was here

clearly favoured over the alkyne mono-annulation to form isoquinolones. Thus, we became attracted to explore the parameters that govern this selectivity.

Scheme 2. Influence of *N*-substitution on C–F activation.

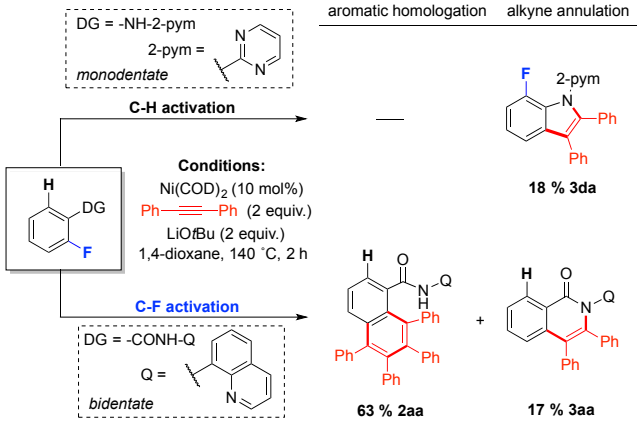

Influence of the electronic effect on the C-F activation. With the optimal conditions for the C–F/C-H activation in hand, we then turned our attention towards the functionalization of the C–F bonds using different fluoroarenes substrates. We performed a reaction using substrate **1b**, which has two fluorides at the *ortho* position of the arene (Table 1, entry 2). In this case we could only obtain 13% of the homologation product **2ba** under otherwise identical conditions, suggesting that the presence of another electron-withdrawing F was not beneficial for the C–F functionalization reaction. The yield of the homologation product did not increase by adding different auxiliary ligands or changing the solvent. In addition, we synthetized substrate **1c** which has two fluorides at the *ortho*- and *meta*- position of the arene to explore the alkyne double insertion via C–F/C–F functionalization. Here, only 12% of the homologation product **2ca** was formed (Table 1, entry 4). Interestingly, using deactivated substrates, no alkyne annulation reaction took place and only aromatic homologation products were observed. The installation of a nitro group at C5 of the quinolone moiety was not productive and only decomposition products were obtained (Table 1, entry 5).

The formation of two distinct products **2** and **3** led us to explore this reactivity further, changing the electronic properties of the alkynes. Initial tests were performed using 1,2-di-*p*-tolyacetylene (Table 2, entry 2) and both products were also formed in a similar ratio (**2ab**/**3ab** ~ 3), although with somewhat lower efficacy. In contrast, C-F activations with electron-deficient *para*-halo-substituted tolanes, yielded equal ratio of the two products (**2ax**/**3ax** ~ 1, entries 3, 4 and 5). This increment in the alkyne mono-annulation products suggests that the presence of electron-withdrawing moieties favour the reductive elimination after the first alkyne insertion.[44-46] To address this point, we decided to study stronger electron-withdrawing-groups (EWG), such as -C(O)Me and -CF_3 in the *para*-position. To our delight, the aromatic homologation reaction was completely suppressed, exclusively obtaining the alkyne mono-annulation products in a 36 % for **3af** (entry 6) and a 83 % for **3ag** (entry 7), respectively.

Table 1. C-F functionalization using different polyfluoroarenes.

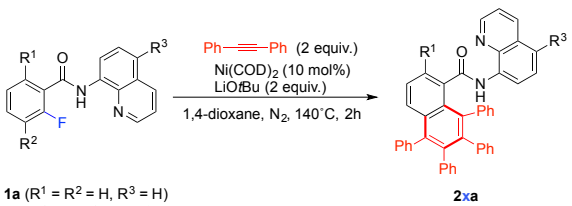

1a (R^1 = R^2 = H, R^3 = H)
1b (R^1 = F, R^2 = H, R^3 = H)
1c (R^1 = H, R^2 = F, R^3 = H)
1e (R^1 = R^2 = H, R^3 = NO_2)

2xa

Entry	R^1	R^2	R^3	Yield (%) of 2xa[a]
1[b]	H	H	H	63 % **2aa**
2	F	H	H	13 % **2ba**
3[c]	F	H	H	34 % **2ba**
4[d]	H	F	H	12 % **2ca**
5[e]	H	H	NO_2	traces **2ea**

[a] Yield calculated from ^{1}H-NMR of crude reaction mixture using 1,3,5-trimethoxybenzene as internal standard. [b] 17% of alkyne annulation product **3aa**. [c] 16 h. [d] Other minor products were detected. [e] Conv = 63%.

Table 2. C-F functionalization using different symmetric alkynes.

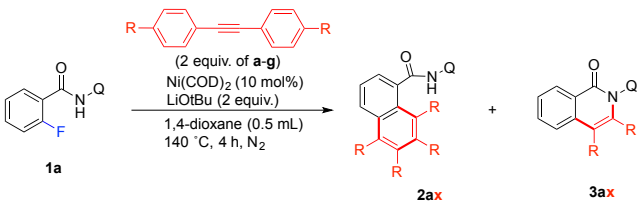

Entry	R'	Yield of 2ax[a]	Yield of 3ax[a]	Total yield
1[b]	H	63 % **2aa** (60 %)	17 % **3aa** (11 %)	80 %
2	Me	40 % **2ab** (40 %)	14 % **3ab** (6 %)	54 %
3	F	40 % **2ac** (36 %)	43 % **3ac** (34 %)	83 %
4	Cl	34 % **2ad** (30 %)	39 % **3ad** (29 %)	73 %
5	Br	37 % **2ae** (25 %)	37 % **3ae** (34 %)	74 %
6	MeC(O)	-	36 % **3af** (22 %)	36 %
7	CF_3	-	88 % **3ag** (83 %)	88 %

[a] Yields calculated by ^{1}H NMR spectroscopy using 1,3,5-trimethoxybenzene as internal standard; Isolated yield in parenthesis. [b] 2 h.

The trend observed in Table 2 is clearly visualized in Scheme S2, plotting the observed **2ax**/**3ax** ratios *versus* the Hammett σ_p parameter. These findings showcase the aromatic homologation products being favored (**2ax**) when electron-donor-groups are present, whereas the monoalkyne annulation products (**3ax**) being preferentially formed with electron-withdrawing substituents.

Study the steric effect on C-F activation. This reactivity was also studied using a set of unsymmetrically substituted alkynes. In all cases, both aromatic homologation and alkyne annulation reactions took place, with the former product being clearly preferred. A mixture of two (out of four) aromatic homologation regioisomers was formed (Table 3, entries 1, 2 and 3). Yet, the alkyne mono-annulation product was isolated with the aromatic motif being preferentially proximal to nitrogen.[47] Finally,

when 4-octyne was used (Table 3, entry 4), the alkyne mono-annulation product was not observed, and up to 53% of the aromatic homologation product, **2ak**, was formed instead. Thus, sterically congested alkyl groups disfavour the alkyne mono-annulation product.

Table 3. C–F functionalization using alkyl-aryl and alkyl-alkyl acetylenes.

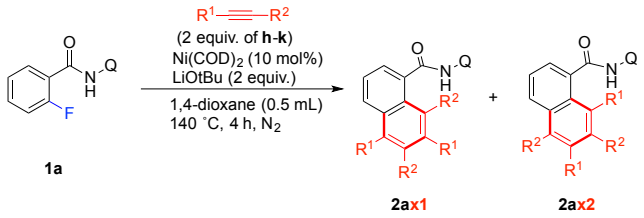

Entry	R^1	R^2	Yield (%) of 2ax [a]	Ratio 2ax1:2ax2 [b]
1[c]	Ph	Me	57 % **2ah** (55 %)	1.6:1.0
2[c]	Ph	Et	70 % **2ai** (49 %)	1.0:1.0
3[c,d]	Ph	Pr	85 % **2aj** (41 %)	1.0:1.2
4[d,e]	Pr	Pr	53 % **2ak** (41 %)	-

[a] Yields determined by ^{1}H-NMR spectroscopy using 1,3,5-trimethoxybenzene as internal standard. Yield **2ax** = **2ax1** + **2ax2**; Isolated yield in parenthesis. [b] Ratio calculated from NMR data. [c] Alkyne mono-annulation products were formed in low quantities (see SI). [d] 8h. [e] Only one aromatic homologation product is possible (**2ak**).

Isolation of Reaction Intermediates. To better understand the observed reactivity, a detailed ^{1}H NMR-monitoring of the reaction of **1a** with diphenylacetylene was performed (Scheme S1). At early stages (10 min), we observed the incipient formation of the products **2aa** and **3aa**. Additionally, we detected the formation of another minor species in the first 30 min of the reaction with a characteristic doublet at 9.06 ppm that subsequently faded away. The *in situ* ^{1}H NMR quantification of the intermediate species between 5 and 15 min accounted for over 80% of the total nickel content in the catalysis, indicating that this species belonged to the productive catalytic cycle.

Encouraged by the possibility of unravelling a key intermediate, we switched from catalytic to stoichiometric conditions and stopped the scaled reaction after 5 min. Upon chromatographic purification, a diamagnetic nickel complex was isolated in 23% yield (**INT4-E-H**). The compound was indeed very stable at room temperature and high-quality crystals allowed unambiguous crystallographic analysis. Strikingly, the XRD structure revealed a square planar nickel(II) complexes with two alkynes being inserted towards a 9-membered nickelocyclic complex (Figure 1). Here, the terminal alkenyl moiety derived from the second inserted alkyne is *trans* to the anionic amide nitrogen. The square planar geometry around the nickel(II) center features the π-coordination of the alkene moiety corresponding to the initially inserted alkyne.[48] The latter nicely explains the extraordinary stability of such an intermediate species without the requirement of additional auxiliary ligands (see below). An analogous reaction with di-*p*-tolylacetylene afforded **INT4-E-Me**, which was likewise fully characterized by NMR spectroscopy. Furthermore, performing the aromatic homologation reaction using the analogous non-fluorinated substrate in the conditions reported by Huang, but at very short reaction times, the formation of the same **INT4-E-H** complex was also achieved (18% yield, Figure 1a and S17).[38] This results suggests that this 9-membered nickelocyclic species is a common intermediate in aromatic homologation reactions, irrespective of being a C-F/C-H or a C-H/C-H activation route. In this line, a competition experiment using equimolar amounts of mono-fluorinated **1a** and the analogous non-fluorinated substrate shows a kinetically preferred C-F over C-H activation due to full consumption of **1a** compared to minimal conversion of the non-fluorinated substrate (Figure 1c). Indeed, a control experiment using only the non-fluorinated substrate in our catalytic conditions produced no aromatic homologation product and stilbene was detected as byproduct, suggesting the implication of a Ni-hydride species (see below).[37-38]

Study of Isolated Ni(II) intermediated in Homologation Reaction. With intermediate **INT4-E-H** in hand, we investigated its evolution to the putative aromatic homologation product (**2aa**) under thermal conditions (Figure 2a), obtaining a modest 23 % yield. Under these conditions (140 °C) and in the presence of 5 equiv. of **1a** and base, a 41% of yield of **2aa** was obtained. This is in line with the requirement of a second aminoquinoline (AQ) chelating unit inducing the *meta* C–H activation at the phenyl ring, which finally renders the aromatic homologation product **2aa** (Figure 2a). In addition, using **INT4-E-H** in 10 mol% under catalytic conditions, its full conversion to **2aa** was obtained (10% yield), although no catalytic turnover was achieved (Figure 2b). In sharp contrast, in the presence of PivOH, product **2aa** was not observed, while up to 46% of the linear alkenylation product **4aa** was obtained (Figure 2a), providing a new strategy towards molecular complexity by C-F activation.

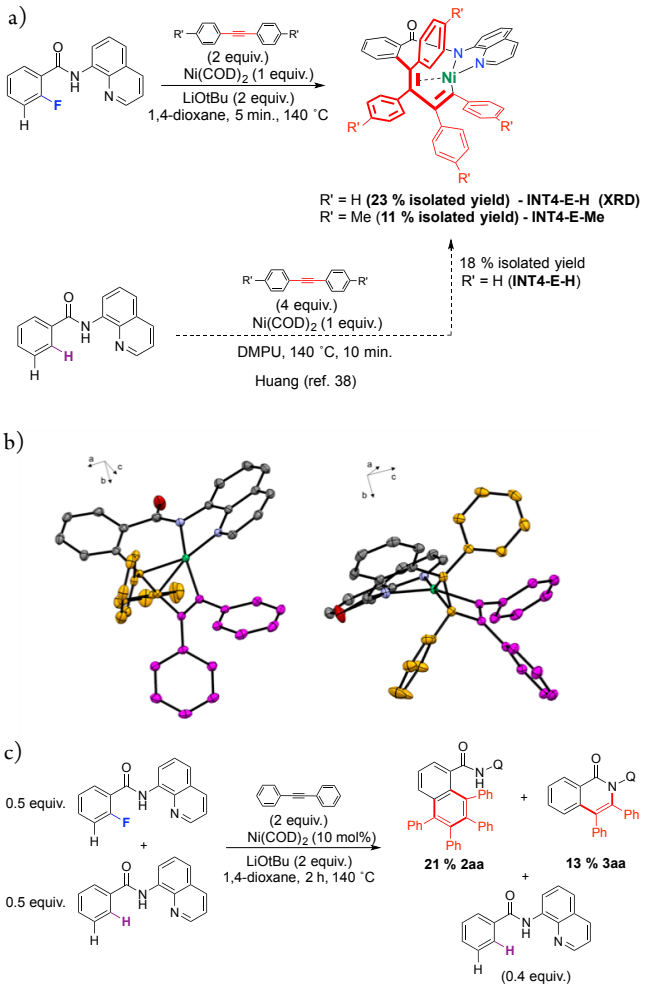

Figure 1. a) Synthesis of **INT4-E-H** complex via C-F/C-H (top) and via C-H/C-H activation previously reported by Huang (yield 18%).[38] b) crystal structure of **INT4-E-H** complex (CCDC 1891021). Selected bond distances [Å]: Ni-C1 2.0411(19), Ni-C2 2.1060(17), Ni-C3 1.8946(16), Ni-N1 1.9209(16), Ni-N2 1.9011(16) (orange: first inserted alkyne in E conformation; magenta: second inserted alkyne in Z conformation; green: nickel(II) center). c) Competition experiment with equimolar amounts of **1a** and the analogous non-fluorinated substrate, obtaining **2aa** and **3aa** products mainly from C-F activation (**1a**, full conversion).

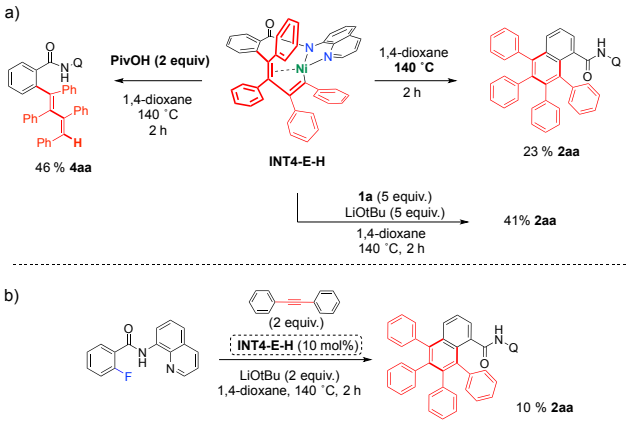

Figure 2. a) Diverting reactivity pathways from **INT4-E-H.** b) Reactivity using **INT4-E-H** as catalyst for the aromatic homologation transformation.

Mechanistic insight. Based on our findings and on the computational study detailed below, a full mechanistic proposal is depicted in Scheme 3. The coordination of deprotonated substrate **1a** with $Ni(COD)_2$ forms the **INT1**, in which the strong C–F bond is cleaved via oxidative addition to generate the nickel(II) intermediate (**INT2**). A detailed DFT study on this step has been performed (Figure 3). The DFT geometry optimizations and frequency calculations have been carried out using the M06-L functional[49] and def2SVP basis set including the solvent effects with the SMD model[50] and the dispersion with Grimme GD3BJ approach. The Gibbs energies obtained were improved with single point calculations at M06-L/def2TZPV including both the solvent and dispersion corrections. A complete description of the computational details of the DFT calculations is given in the supporting information. The results presented in Figure 3 show that the high selectivity of the oxidative addition step towards C-F activation in front C-H activation is due to a) smaller energy barrier for Li^+ Lewis acid assisted C-F activation compared to C-H activation by 4.6 kcal/mol, b) the formation of the hydride-Ni(II) species (**INT2-H**) is strongly endergonic and c) the generation of fluoride-Ni(II) species (**INT2-F**) is clearly exergonic (49.4 kcal/mol more stable than **INT2-H**). Moreover, no alkene or H_2 is formed during the reaction, which is in line with the computational data.

Scheme 3. Global mechanistic proposal. Ni(0) is depicted in purple and Ni(II) in green.

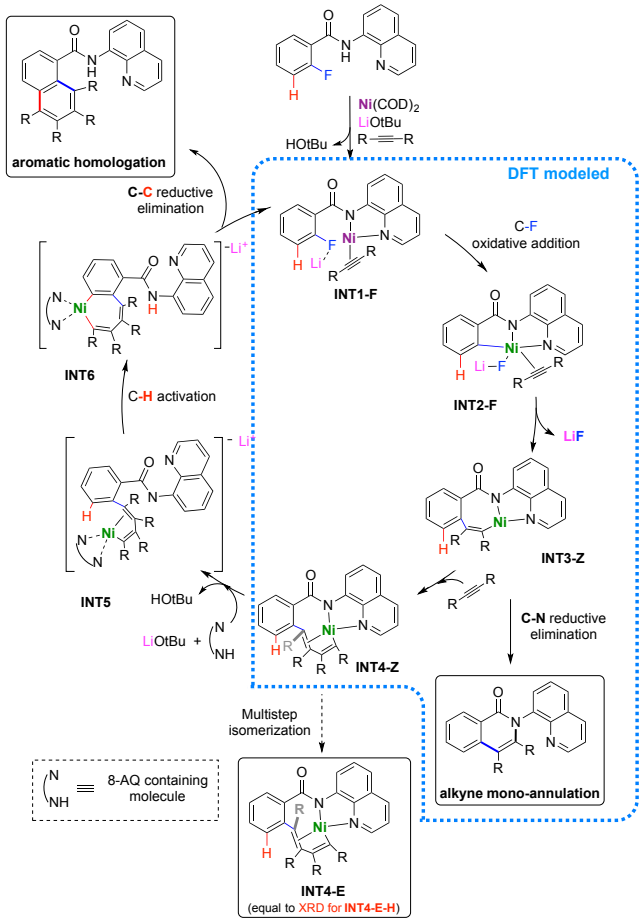

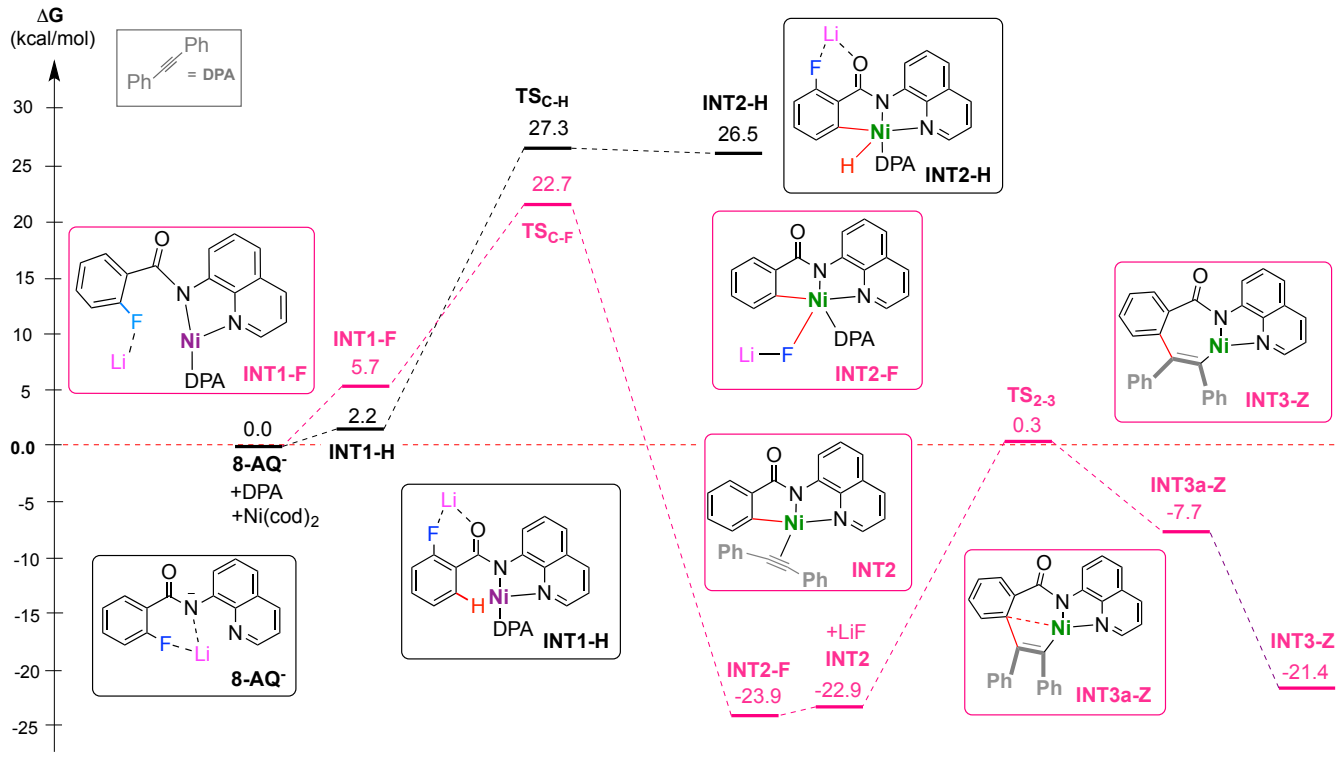

Figure 3. Gibbs Energy profiles for the C-F (pink) versus C-H activation (black) through **INT2-F** and **INT2-H**, respectively, followed by the first DPA insertion at **INT2-F** to form **INT3-Z**. The reaction was modeled by DFT at M06L/Def2TZVP//M06L/Def2SVP level of theory; energies given in kcal/mol.

The role of Li^+ is remarkable since it facilitates the C-F oxidative addition, stabilizes the fluoride-Ni(II) species and is ready to extrude LiF (see TS_{CF} in Figure 4), which formation is one of the driving forces of the reaction. Actually, the reaction does not proceed using *t*BuOK (potassium salt) as base. After the C-F oxidative addition step and extrusion of LiF, the first alkyne insertion (diphenyl acetylene -DPA- was modelled) follows to form **INT3-Z**, with a barrier of 24.2 kcal/mol (Figure 3) (DFT studies clearly indicate that **INT3-Z** isomer is thermodynamically favored compared to **INT3-E**, see below and Figures 5-6).

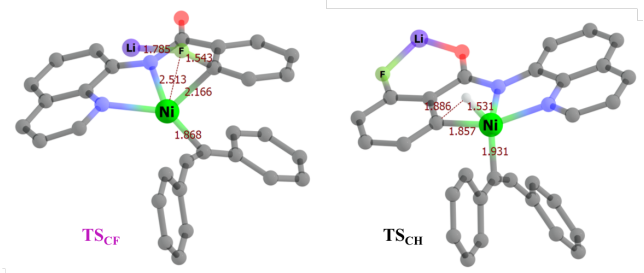

Figure 4. Optimized geometries of **TS_{CF} and TS_{CH}**.

At this point, chemo-divergent behaviour can occur: i) the **INT3-Z** can either undergo reductive elimination to form the alkyne mono-annulation product **3** or ii) a second alkyne insertion into a Ni–C bond proceeds towards **INT4-Z**. When the latter is formed, this can either isomerize to form the **INT4-E** (equivalent to the isolated crystal structure **INT4-E-H**), which is more stable than **INT4-Z** (see below), or it can further react towards the synthesis of the homologation product.

The experimental results suggest that additional presence of 8-AQ-motifs either in the substrate or the products, facilitate the activation of the meta C–H bond by stabilizing the nickel(II) center to give the final homologation product (**INT5** and **INT6**). The presence of EWG on the alkyne triggers the chemo-divergent transformation of **INT3-Z** to the alkyne mono-annulation product, instead of the aromatic homologation product.

The insertion of the first alkyne may lead to two different **INT3** isomers, **INT3-Z** and **INT3-E** (Figure 5), which are differentiated by the stereochemistry of the C-C double bond from the first inserted alkyne in Z (**INT3-Z**) or in E conformation (**INT3-E**).[51] The latter is 6.0 kcal/mol less stable than the former. The formation of **INT4-E** (-19.3 kcal/mol), which has exactly the same geometry as the crystal structure of **INT4-E-H** depicted in Figure 1, requires overcoming **TS-$E_{3\text{-}4}$** (33.4 kcal/mol). However, we found a far more kinetically favourable mechanism involving the first inserted alkyne in a Z conformation, which transition state Gibbs energy (**TS-$Z_{3\text{-}4}$**) is 21.5 kcal/mol lower than **TS-$E_{3\text{-}4}$** (Figure 5). Importantly, the product obtained **INT4-Z** (-8.1 kcal/mol) is 11.2 kcal/mol less stable than **INT4-E**. The experimental crystallization of **INT4-E-H** was mirrored by its strong thermodynamic stability found in the calculations, which is the driving force of a multistep isomerization of **INT4-Z** upon isolation as solid. In addition, detailed analysis of geometry of the Ni(II) center for optimized **INT4-Z** and **INT4-E** structures (by checking the dihedral angle between the atoms directly bonded to the metal), showed that the E-isomer is significantly less distorted from the square-planarity (dihedral angle 23.3º) than the Z-isomer (50.2º), thereby explaining the thermodynamic stability of **INT4-E** compared to **INT4-Z** (Figure 6).

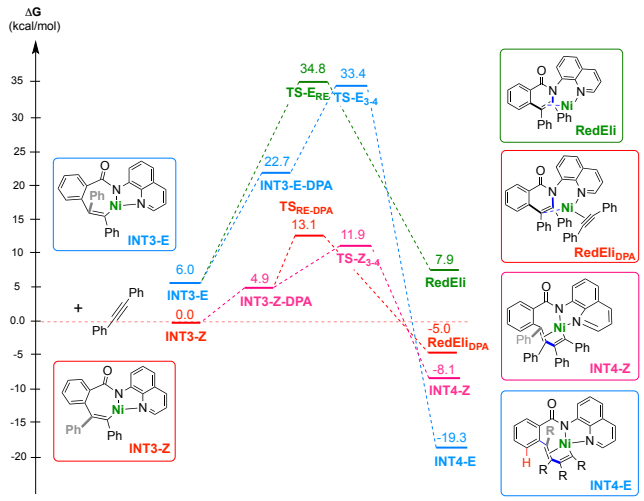

Figure 5. Gibbs Energy profiles for the transition from the monoalkyne intermediates (**INT3-E** or **INT3-Z**) to the double inserted alkyne compounds **INT4-E** (in blue) or **INT4-Z** (in pink), as well as the pathways for the intramolecular alkyne mono-annulation from **INT3-E** (in green) and the annulation from **INT3-Z** with a second DPA coordinated to the metal (in red). The reaction was modeled by DFT at M06L/Def2TZVP//M06L/Def2SVP level of theory; energies given in kcal/mol.

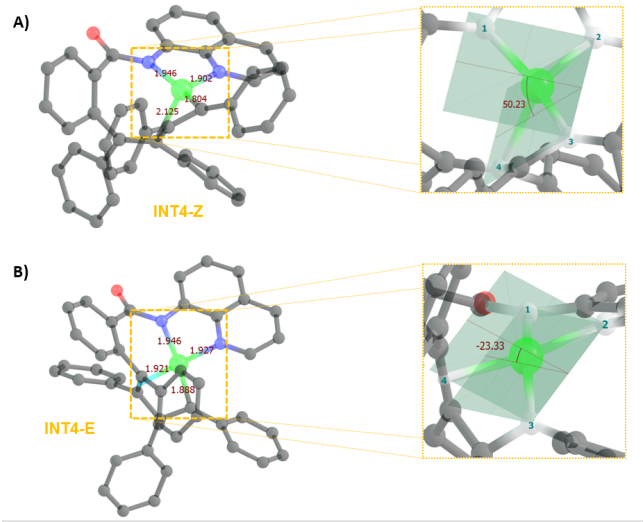

Figure 6. Optimized geometries of a) **INT4-Z** and b) **INT4-E**. The enlarged section highlights the distortion of the square planarity on the complex by measuring the dihedral angle N1N2C3C4. Atom-color code: C grey, N blue, O red, Ni green (Hydrogen atoms have been omitted for clarity).

The small energy barriers for the C-F oxidative addition, first alkyne insertion and second alkyne insertion (< 24 kcal/mol), together with the isolation of the double-alkyne-inserted nickelocyclic intermediate species, are in agreement with the rate-determining step being later than the insertion of the second alkyne.

Regarding the computed pathway leading to the alkyne mono-annulation products (Figure 5), the most kinetically favourable pathway involves a second molecule of acetylene coordinated to **INT3-Z**. It evolves through a reductive elimination transition state, **TS-Z$_{RE-DPA}$** (13.11 kcal/mol), which is only slightly above of **TS-Z$_{3-4}$** by 1.2 kcal/mol (Figure 7). This small Gibbs energy difference agrees with the experimental formation both aromatic homologation and alkyne mono-annulation products, being the former one preferred. When *p*-CF_3-substituted alkyne is used, the Gibbs energy difference between the transition state of the second alkyne insertion, **CF$_3$-TS-Z$_{3-4}$** (13.4 kcal/mol) and the intramolecular reductive elimination, **CF$_3$-TS-Z$_{RE-DPA}$** (14.0 kcal/mol) is reduced to 0.6 kcal/mol, in agreement with the experimental trend observed when EWG are present (see Figure S21).

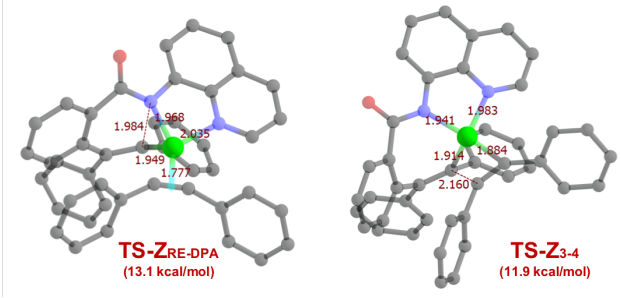

Figure 7. Optimized geometries of **TS-Z$_{RE-DPA}$** and **TS-Z$_{3-4}$**.

CONCLUSIONS

In summary, we have developed a nickel-catalyzed C–F functionalization with internal alkynes to form either alkyne mono-annulation or aromatic homologation products in a chemo-divergent manner. Electronic properties on the fluoroarene and on the alkynes allowed to selectively guide the reaction manifold. The selectivity for C-F over C-H activation is based on a lower transition state and exergonic step, as ascertained by DFT analysis, highlighting the crucial role of the Li^+ in assisting the removal of the fluoride anion. A key unprecedented nickelocyclic species featuring a double-inserted alkyne was isolated and crystalized, unravelling the mechanistic pathway to the aromatic homologation product by challenging double C-F/C-H activation, which is also found for previously reported C-H/C-H aromatic homologations. These findings should prove instrumental as a mechanistic guidance for further transition-metal-catalyzed aromatic homologation reactions.

ASSOCIATED CONTENT

Supporting Information.

Detailed spectroscopic characterization of all compounds is included, optimization details, experimental details of catalytic reactions, experimental details of stoichiometric reactions for the formation of **INT4-E-H** and **INT4-E-Me** and also computational details. Crystallographic data for **INT4-E-H** (CCDC-1891021) is provided.

AUTHOR INFORMATION

Corresponding Author

*lutz.Ackermann@chemie.uni-goettingen.de
*xavi.ribas@udg.edu

Notes

The authors declare no competing financial interest.

Crystallographic data for **INT4-E-H** (CCDC-1891021) can be obtained free of charge from the Cambridge Crystallographic Data Centre via www.ccdc.cam.ac.uk/data_request/cif.

ACKNOWLEDGMENT

This work was financially supported by grants from the European Research Council (ERC-2011-StG-277801 to XR), the DFG (Gottfried-Wilhelm-Leibniz award to LA), MICINN (CTQ2016-77989-P to XR), and Generalitat de Catalunya (2017SGR264). XR is thankful for an

ICREA Acadèmia award. We thank COST Action CHAOS (CA15106) and Dr. L. Gómez and STR from UdG for technical support.

REFERENCES

1. Böhm, H.-J.; Banner, D.; Bendels, S.; Kansy, M.; Kuhn, B.; Müller, K.; Obst-Sander, U.; Stahl, M., Fluorine in Medicinal Chemistry. *ChemBioChem* **2004,** *5*, 637-643.
2. Müller, K.; Faeh, C.; Diederich, F., Fluorine in Pharmaceuticals: Looking Beyond Intuition. *Science* **2007,** *317*, 1881-1886.
3. Purser, S.; Moore, P. R.; Swallow, S.; Gouverneur, V., Fluorine in medicinal chemistry. *Chem. Soc. Rev.* **2008,** *37*, 320-330.
4. Wang, J.; Sánchez-Roselló, M.; Aceña, J. L.; del Pozo, C.; Sorochinsky, A. E.; Fustero, S.; Soloshonok, V. A.; Liu, H., Fluorine in Pharmaceutical Industry: Fluorine-Containing Drugs Introduced to the Market in the Last Decade (2001–2011). *Chem. Rev.* **2014,** *114*, 2432-2506.
5. Sun, A. D.; Love, J. A., Cross coupling reactions of polyfluoroarenes via C-F activation. *Dalton Trans.* **2010,** *39*, 10362-10374.
6. Amii, H.; Uneyama, K., C−F Bond Activation in Organic Synthesis. *Chem. Rev.* **2009,** *109*, 2119-2183.
7. Ahrens, T.; Kohlmann, J.; Ahrens, M.; Braun, T., Functionalization of Fluorinated Molecules by Transition-Metal-Mediated C–F Bond Activation To Access Fluorinated Building Blocks. *Chem. Rev.* **2015,** *115*, 931-972.
8. Kiso, Y.; Tamao, K.; Kumada, M., Effects of the nature of halides on the alkyl group isomerization in the nickel-catalyzed cross-coupling of secondary alkyl Grignard reagents with organic halides. *J. Organomet. Chem.* **1973,** *50*, C12-C14.
9. Ackermann, L.; Born, R.; Spatz, J. H.; Meyer, D., Efficient Aryl–(Hetero)Aryl Coupling by Activation of C-Cl and C-F Bonds Using Nickel Complexes of Air-Stable Phosphine Oxides. *Angew. Chem. Int. Ed.* **2005,** *44*, 7216-7219.
10. Yoshikai, N.; Mashima, H.; Nakamura, E., Nickel-Catalyzed Cross-Coupling Reaction of Aryl Fluorides and Chlorides with Grignard Reagents under Nickel/Magnesium Bimetallic Cooperation. *J. Am. Chem. Soc.* **2005,** *127*, 17978-17979.
11. Yoshikai, N.; Matsuda, H.; Nakamura, E., Hydroxyphosphine Ligand for Nickel-Catalyzed Cross-Coupling through Nickel/Magnesium Bimetallic Cooperation. *J. Am. Chem. Soc.* **2009,** *131*, 9590-9599.
12. Wang, J.-R.; Manabe, K., High Ortho Preference in Ni-Catalyzed Cross-Coupling of Halophenols with Alkyl Grignard Reagents. *Org. Lett.* **2009,** *11*, 741-744.
13. Ackermann, L.; Wechsler, C.; Kapdi, A. R.; Althammer, A., Air-Stable Diaminophosphine Sulfides as Preligands for Nickel-Catalyzed Cross-Couplings of Unactivated Fluoro(hetero)arenes. *Synlett* **2010,** *2010*, 294-298.
14. Nakamura, Y.; Yoshikai, N.; Ilies, L.; Nakamura, E., Nickel-Catalyzed Monosubstitution of Polyfluoroarenes with Organozinc Reagents Using Alkoxydiphosphine Ligand. *Org. Lett.* **2012,** *14*, 3316-3319.
15. Guo, W.-J.; Wang, Z.-X., Cross-Coupling of ArX with ArMgBr Catalyzed by N-Heterocyclic Carbene-Based Nickel Complexes. *J. Org. Chem.* **2013,** *78*, 1054-1061.
16. O'Neill, M. J.; Riesebeck, T.; Cornella, J., Thorpe–Ingold Effect in Branch-Selective Alkylation of Unactivated Aryl Fluorides. *Angew. Chem. Int. Ed.* **2018,** *57*, 9103-9107.
17. Schaub, T.; Backes, M.; Radius, U., Catalytic C−C Bond Formation Accomplished by Selective C−F Activation of Perfluorinated Arenes. *J. Am. Chem. Soc.* **2006,** *128*, 15964-15965.
18. Sun, A. D.; Love, J. A., Nickel-Catalyzed Selective Defluorination to Generate Partially Fluorinated Biaryls. *Org. Lett.* **2011,** *13*, 2750-2753.
19. Tobisu, M.; Xu, T.; Shimasaki, T.; Chatani, N., Nickel-Catalyzed Suzuki–Miyaura Reaction of Aryl Fluorides. *J. Am. Chem. Soc.* **2011,** *133*, 19505-19511.
20. Zhou, J.; Berthel, J. H. J.; Kuntze-Fechner, M. W.; Friedrich, A.; Marder, T. B.; Radius, U., NHC Nickel-Catalyzed Suzuki–Miyaura Cross-Coupling Reactions of Aryl Boronate Esters with Perfluorobenzenes. *J. Org. Chem.* **2016,** *81*, 5789-5794.
21. Ho, Y. A.; Leiendecker, M.; Liu, X.; Wang, C.; Alandini, N.; Rueping, M., Nickel-Catalyzed Csp2–Csp3 Bond Formation via C–F Bond Activation. *Org. Lett.* **2018,** *20*, 5644-5647.
22. Yu, D.; Shen, Q.; Lu, L., Selective Palladium-Catalyzed C–F Activation/Carbon–Carbon Bond Formation of Polyfluoroaryl Oxazolines. *J. Org. Chem.* **2012,** *77*, 1798-1804.
23. Yu, D.; Wang, C.-S.; Yao, C.; Shen, Q.; Lu, L., Nickel-Catalyzed α-Arylation of Zinc Enolates with Polyfluoroarenes via C–F Bond Activation under Neutral Conditions. *Org. Lett.* **2014,** *16*, 5544-5547.
24. Guimond, N.; Gouliaras, C.; Fagnou, K., Rhodium(III)-Catalyzed Isoquinolone Synthesis: The N–O Bond as a Handle for C–N Bond Formation and Catalyst Turnover. *J. Am. Chem. Soc.* **2010,** *132*, 6908-6909.
25. Ackermann, L.; Lygin, A. V.; Hofmann, N., Ruthenium-Catalyzed Oxidative Annulation by Cleavage of C-H/N-H Bonds. *Angew. Chem. Int. Ed.* **2011,** *50*, 6379-6382.
26. Shiota, H.; Ano, Y.; Aihara, Y.; Fukumoto, Y.; Chatani, N., Nickel-Catalyzed Chelation-Assisted Transformations Involving Ortho C–H Bond Activation: Regioselective Oxidative Cycloaddition of Aromatic Amides to Alkynes. *J. Am. Chem. Soc.* **2011,** *133*, 14952-14955.
27. Cera, G.; Haven, T.; Ackermann, L., Iron-catalyzed C–H/N–H activation by triazole guidance: versatile alkyne annulation. *Chem. Commun.* **2017,** *53*, 6460-6463.
28. Tian, C.; Massignan, L.; Meyer, T. H.; Ackermann, L., Electrochemical C−H/N−H Activation by Water-Tolerant Cobalt Catalysis at Room Temperature. *Angew. Chem. Int. Ed.* **2018,** *57*, 2383-2387.
29. Song, W.; Ackermann, L., Nickel-catalyzed alkyne annulation by anilines: versatile indole synthesis by C–H/N–H functionalization. *Chem. Commun.* **2013,** *49*, 6638-6640.
30. Stuart, D. R.; Bertrand-Laperle, M.; Burgess, K. M. N.; Fagnou, K., Indole Synthesis via Rhodium Catalyzed Oxidative Coupling of Acetanilides and Internal Alkynes. *J. Am. Chem. Soc.* **2008,** *130*, 16474-16475.
31. Ackermann, L., Carboxylate-Assisted Ruthenium-Catalyzed Alkyne Annulations by C–H/Het–H Bond Functionalizations. *Acc. Chem. Res.* **2014,** *47*, 281-295.
32. Shi, Z.; Zhang, C.; Li, S.; Pan, D.; Ding, S.; Cui, Y.; Jiao, N., Indoles from Simple Anilines and Alkynes: Palladium-Catalyzed C-H Activation Using Dioxygen as the Oxidant. *Angew. Chem. Int. Ed.* **2009,** *48*, 4572-4576.
33. Le Bras, J.; Muzart, J., Dehydrogenative Heck Annelations of Internal Alkynes. *Synthesis* **2014,** *46*, 1555-1572.
34. Fukutani, T.; Hirano, K.; Satoh, T.; Miura, M., Synthesis of Highly Substituted Acenes through Rhodium-Catalyzed Oxidative Coupling of Arylboron Reagents with Alkynes. *J. Org. Chem.* **2011,** *76*, 2867-2874.
35. Pham, M. V.; Cramer, N., Aromatic Homologation by Non-Chelate-Assisted RhIII-Catalyzed C-H Functionalization of Arenes with Alkynes. *Angew. Chem. Int. Ed.* **2014,** *53*, 3484-3487.
36. Martínez, Á. M.; Echavarren, J.; Alonso, I.; Rodríguez, N.; Gómez Arrayás, R.; Carretero, J. C., RhI/RhIII catalyst-controlled divergent aryl/heteroaryl C–H bond functionalization of picolinamides with alkynes. *Chem. Sci.* **2015,** *6*, 5802-5814.
37. Misal Castro, L. C.; Obata, A.; Aihara, Y.; Chatani, N., Chelation-Assisted Nickel-Catalyzed Oxidative Annulation via Double C−H Activation/Alkyne Insertion Reaction. *Chem. Eur. J.* **2016,** *22*, 1362-1367.
38. He, Z.; Huang, Y., Diverting C–H Annulation Pathways: Nickel-Catalyzed Dehydrogenative Homologation of Aromatic Amides. *ACS Catal.* **2016,** *6*, 7814-7823.
39. Gandeepan, P.; Müller, T.; Zell, D.; Cera, G.; Warratz, S.; Ackermann, L., 3d Transition Metals for C–H Activation. *Chem. Rev.* **2018**.
40. Eisenstein, O.; Milani, J.; Perutz, R. N., Selectivity of C–H Activation and Competition between C–H and C–F Bond Activation at Fluorocarbons. *Chem. Rev.* **2017,** *117*, 8710-8753.
41. Ghorai, D.; Finger, L. H.; Zanoni, G.; Ackermann, L., Bimetallic Nickel Complexes for Aniline C–H Alkylations. *ACS Catal.* **2018,** *8*, 11657-11662.
42. Grigorjeva, L.; Daugulis, O., Cobalt-Catalyzed, Aminoquinoline-Directed C(sp2)-H Bond Alkenylation by Alkynes. *Angew. Chem. Int. Ed.* **2014,** *53*, 10209-10212.
43. Bennett, M. A.; Wenger, E., The Reactivity of Complexes of Nickel(0) and Platinum(0) Containing Benzyne and Related Small-Ring Alkynes. *Chem. Ber.* **1997,** *130*, 1029-1042.
44. Johnson, J. B.; Rovis, T., More than Bystanders: The Effect of Olefins on Transition-Metal-Catalyzed Cross-Coupling Reactions. *Angew. Chem. Int. Ed.* **2008,** *47*, 840-871.
45. Huang, C.-Y.; Doyle, A. G., Electron-Deficient Olefin Ligands Enable Generation of Quaternary Carbons by Ni-Catalyzed Cross-Coupling. *J. Am. Chem. Soc.* **2015,** *137*, 5638-5641.
46. Yamamoto, T.; Yamamoto, A.; Ikeda, S., Organo (dipyridyl) nickel complexes. I. Stability and activation of the alkyl-nickel bonds of dialkyl

(dipyridyl) nickel by coordination with various substituted olefins. *J. Am. Chem. Soc.* **1971,** *93*, 3350-3359.
47. Meyer, T. H.; Oliveira, J. C. A.; Sau, S. C.; Ang, N. W. J.; Ackermann, L., Electrooxidative Allene Annulations by Mild Cobalt-Catalyzed C–H Activation. *ACS Catal.* **2018,** *8*, 9140-9147.
48. Denninger, U.; Schneider, J. J.; Wilke, G.; Goddard, R.; Krömer, R.; Krüger, C., Transition metal complexes: VIII. An unusual rearrangement of a butadienyl ligand via cyclometallation. *J. Organomet. Chem.* **1993,** *459*, 349-357.
49. Zhao, Y.; Truhlar, D. G., A new local density functional for main-group thermochemistry, transition metal bonding, thermochemical kinetics, and noncovalent interactions. *J. Chem. Phys.* **2006,** *125*, 194101.
50. Marenich, A. V.; Cramer, C. J.; Truhlar, D. G., Universal solvation model based on solute electron density and on a continuum model of the solvent defined by the bulk dielectric constant and atomic surface tensions. *J. Phys. Chem. B* **2009,** *113*, 6378-6396.
51. The possibility that a second AQ-containing substrate might coordinate at INT3-Z as proposed in the literature (see ref. 37)was discarded for the endergonic nature of the adduct formed with 1a-Li, as ascertained by DFT calculations (see SI).

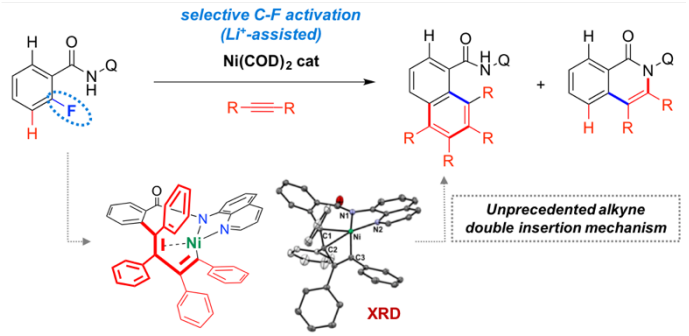
selective C-F activation
(Li+-assisted)
Ni(COD)2 cat
R—≡—R
Unprecedented alkyne
double insertion mechanism
XRD